Detection of Metallic Foreign Objects and Electric Vehicles Using Auxiliary Coil Sets for Dynamic Inductive Power Transfer Systems

Shi, Wenli; Grazian, Francesca; Dong, Jianning; Soeiro, Thiago Batista; Bauer, Pavol

DOI
10.1109/ISIE45063.2020.9152424

Publication date
2020

Document Version
Final published version

Published in
2020 IEEE 29th International Symposium on Industrial Electronics (ISIE)

Detection of Metallic Foreign Objects and Electric Vehicles Using Auxiliary Coil Sets for Dynamic Inductive Power Transfer Systems

Wenli Shi, Francesca Grazian, Jianning Dong, Thiago Batista Soeiro, and Pavol Bauer
Dept. Electrical Sustainable Energy, DCE&S group
TU Delft, Mekelweg 04, 2628 CD, Delft, the Netherlands
E-mail: W.Shi-3, F.Grazian, J.Dong-4, T.BatistaSoeiro, P.Bauer@tudelft.nl

***Abstract*—This paper proposes a new method of electric vehicles detection (EVD) and foreign objects detection (FOD) for dynamic inductive power transfer (DIPT) systems. The proposed detection method applies both passive coil sets (PCSs) and active coil sets (ACSs) to achieve both EVD and FOD with a high detection sensitivity. The operation mechanisms and design of the detection coil sets topology and resonant circuits are elaborated. Finally, both circuit and magnetic field simulation are carried out. The results verify the feasibility and sensitivity of the proposed detection method.**

Keywords—dynamic inductive power transfer, foreign objects detection, electric vehicles detection, resonant circuits.

I. INTRODUCTION

The inductive power transfer (IPT) technique has gained extensive attention as it enables energy transfer over a large air gap. Since there is no mechanical contact between the primary and secondary charging pads, the IPT system can be sealed, which makes it resistive to dust, water, and chemicals. With a tradeoff between the power transfer distance and efficiency, the IPT technique is increasingly popularized in both the low-power devices like biomedical implants, smartphones and the high-power equipment including factory automation and electric vehicles (EVs).

Dynamic IPT (DIPT) system makes it possible to charge EVs while this is on the move across the road. This technique can reduce the EV battery size and extend its driving range. Typically, transmitters are buried along the road in the form of segmented pads or elongated tracks. If all transmitters are powered, the uncoupled transmitters produce a large leakage magnetic field which may be exposed to pedestrians and pose a threat to human safety. To determine the ON/OFF state of each transmitter, the DIPT system is required to detect the position of the EVs. Besides, foreign objects (FOs) may be found on the top of the transmitter, which results in extra power losses reducing the power transfer efficiency of the system as well as they pose as fire hazards. Therefore, DIPT systems are also required to detect FOs.

There are mainly two EV detection (EVD) approaches based on electrical circuits. One is called reflexing segmentation which utilizes the equivalent reflected impedance to the transmitter side [1]. In the absence of the receiver, the primary input impedance has a large reactance allowing minimal current circuiting in the resonant tank. This approach requires no sensor device at a price of efficiency reduction caused by the coil copper losses due to the circulating reactive power. The other approach applies an auxiliary source coil beneath the receiver and auxiliary detection coil sets on top of the transmitter [2]. The auxiliary source coil has a power supply whose frequency is several times higher than 85 kHz. By measuring the induced voltage on the detection coil sets, EVs can be detected when they are in the vicinity of the transmitter.

Regarding FO detection (FOD), if the object is a metallic FO (MFO), such as canned drinks and coins, eddy current is generated within the object when the transmitters are energized. The eddy current produces heat which may cause overheating or even a fire, and additionally the MFO generates a magnetic field counteracting the source field. Therefore, system parameters like coil inductance and mutual inductance changes due to the presence of MFOs. As a consequence, the system performances, including the current waveform, efficiency and effective power will degrade. Thus, it is essential to detect MFOs during the operation and remove them or temporarily shuttdown the transmitters nearby.

In the field of inductive EV charging, a few methods to detect MFOs are reported, which can be classified into two types. The first method collects the inherent changes of the IPT system resulted from MFOs.This involves the measurement of the variations of system parameters, such as the coil quality factor [3], resonant or cut-off frequency [4], and power efficiency [5]. In [5], the efficiency with and without metal objects are compared. If efficiency deviates from the rated value to a certain degree, the presence of the MFO is reported. This method has been proved to be cost-effective and simple, but its application is limited to low power IPT applications [6]. This occurs because in high power applications the losses caused by the presence of MFO is comparatively low in relation to the active power.

The other type of FOD method applies active or passive auxiliary coil sets. The passive coil sets (PCS) measure the induced voltage caused by the magnetic field produced by the eddy current within the MFO [7]–[9]. Thus, this approach requires excitation of the transmitter and zero couplings between the transmitter and the detection coil sets. Overlapped detection coil is developed by WiTricity to sense the imbalanced voltage resulted from metallic objects [8]. When there is no metallic object, the detection voltage is zero. In order to remove the blind zone at every intersection point of the coils, an extra set of detection coils is added as interleaved ones. Detection method applying non-overlapped coils is presented in [7]. Two coil arrays are configured longitudinally and laterally. This structure enables the detection device to determine the presence of metallic objects by the induced voltage difference. However, PCS detection fails when the total magnetic flux of the MFO is zero. In the

The results presented in this paper are developed in the framework of the 16ENG08 MICEV Project. The latter received funding from the EMPIR programme co-financed by the Participating States and from the European Union's Horizon 2020 research and innovation programme.

978-1-7281-5635-4/20/$31.00 ©2020 IEEE

case that the thin MFO is placed onto the center of the Double-D (DD) charging pad, PCSs cannot detect the MFO.

The active coil sets (ACS) measures the impedance variation caused by the MFOs [10]. In [10], a parallel capacitor is adopted to compensate for a detection coil set, because the input impedance of the parallel resonant tank decreases dramatically when the operation point deviates from the resonance. The self-inductance change of the detection coil can be amplified and reflected by the reduction of the input impedance. To cover the surface of the transmitter pad, multiple ACSs are required. However, if there are more than two ACSs working, the coupling between these ACSs will detune the resonant circuit. Thus, coordinating switches are required to avoid the simultaneous operation of multiple ACSs, which is costy and complex.

This paper proposes a new detection method achieving both EVD and FOD. The advantages include zero-blind-zone FOD without switches controlling ACSs, and integrated EVD using the same set of device. In the proposed method, ACSs are used to eliminate the typical blind zone of the PCSs. Meanwhile, PCSs are applied to cover the detection area which is out of the boundary of ACSs. In the following part of this paper, the mechanisms of EVD and FOD are explained. Then, the topologies of the detection coil sets and its detection resonant circuit are analyzed. Finally, simulations are implemented to verify the feasibility of the proposed detection method.

II. Principles of EVs and MFOs Detection

The detection methods discussed in this paper are based on the sensing of the magnetic field variations resulted from the intrusion of MFOs or EVs using different coil sets. The operation principles of different detection methods are introduced in this section.

A. Passive detection coil sets

When a MFO is placed in a changing magnetic field, the distribution of the magnetic field changes because of the induced eddy current. As shown in Fig. 1, if an open-circuit passive coil set (PCS) is placed on top of the source coil, a variation of its induced voltage could be observed due to the intrusion of the MFO.

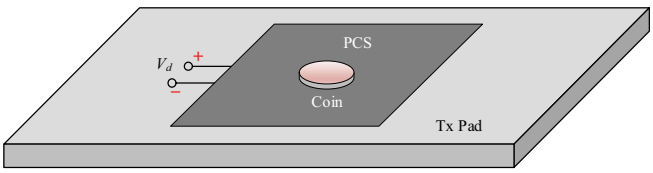

Fig. 1. PCSs detection mechanisms

The sensitivity S_{PDCS} can be calculated as

$$S_{PCS} = \left|\frac{V_d - V_d'}{V_d'}\right| \quad (1)$$

where V_d and V_d' are the PCS induced voltages with and without the presence of the MFO, repectively. When the PCS is coupled with the transmitter (Tx) pad, V_d' may be far larger than V_d, especially in high power applications, and the detection may not work properly. In order to gain a higher S_{PCS}, the PCS is required to be decoupled from the Tx pad. For example, a bipolar PCS is decoupled from a unipolar Tx pad while their centres are overlapped. On the other hand, the sensitivity could also be increased by shrinking the size of the PCS. Therefore, instead of utilizing one large PSC, multiple smaller PSCs are applied to cover the surface of the Tx pad [7], [9], [11].

B. Active detection coil sets

In the ACS based FOD method, an ACS is placed on the detection surface, as shown in Fig. 2 . Due to the coupling between the MFO and the source coil, the equivalent self-inductance L_1 and resistance R_1 of the source coil changes [12]. It is proved that the MFO causes an increment of the equivalent resistance and a decrement of the equivalent self-inductance of the source coil. Therefore, the variation of the source coil impedance could reflect the intrusion of the MFO. However, the impact of small MFOs like coins on the source coil impedance is limited, and a way to amplify the source coil impedance variation is to connect capacitors to the source coil and form a resonant circuit where the input impedance Z_d is sensitive to the resonant operation point.

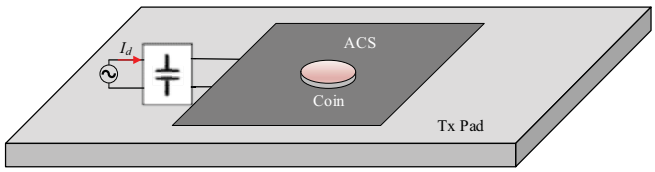

Fig. 2. ACSs detection mechanisms

The ACSs detection method commonly adopts capacitors to build a resonant tank with the source coil and an AC source to power the ACSs, as presented in Fig. 2. The input current of the resonant circuit I_d changes as Z_d varies due to the MFO. Therefore, I_d is measured to identify whether there is a MFO or not. The sensitivity of ACSs detection S_{ACS} is defined as

$$S_{ACS} = \left|\frac{I_d' - I_d}{I_d'}\right| = G_r \left|\frac{L_1' - L_1}{L_1'}\right| = G_r \frac{M_f^2 \omega^2 L_f}{L_1'(L_f^2 \omega^2 + R_f^2)} \quad (2)$$

where G_r is the gain coefficient determined by the resonant circuit, L_1 and L_1' are the equivalent inductance of the ACS with and without MFO, L_f and R_f are the equivalent self-inductance and resistance of the MFO, M_f is the mutual inductance between the MFO and ACS. The selection of the resonant circuit will be discussed in the next section. It can be seen that S_{ACS} is proportional to M_f and reversely proportional to L_1'. The increment of M_f and decrement of L_1' can be realized by shrinking the size of the ACS. However, ACSs are powered by AC current which does not exist in PCSs, and one ACS may couple with another ACS. If multiple ACSs are deployed to cover the area of the Tx pad, the coupling among ACSs may mistune the resonant circuits. As a consequence, the detection method fails. Meanwhile, ACSs are also required to be decoupled with the Tx pad. In the case that the ACS is connected to a capacitor in parallel, extra reactive power will be introduced to the DIPT system and the power transfer efficiency drops as well. One solution is to adopt coordinating switches to each ACS resonant circuit, such that there is only one ACS resonant circuit working each time [10].

C. Electric Vehicle Detection

Similar with FOD methods, EVD can also be realized by applying auxiliary coil sets placed onto the charging pads. To detect the EV, an EV source coil (EVSC) is mounted below the receiver (Rx) pad and EVD coil sets (EVDCS) are installed onto the Tx pad, as shown in Fig. 3. The EVSC is excited by a power supply with a frequency several times higher than the rated charging frequency of 85 kHz. When the EV moves along the x-axis, an induced voltage across the EVDCS V_{EV} can be observed. By measuring V_{EV}, the EV can

be detected when the distance between the Tx and Rx pads in the x-axis is small enough.

The mutual inductance M_{EVD} between the EVSC and EVDCS changes as shown in Fig. 4. M_{EVD} peaks when Tx and Rx are perfectly aligned. However, the peak value is relatively small which makes it difficult to measure V_{EV}. In order to amplify V_{EV}, capacitors are connected to the EVDCS to build a series resonant circuit. V_{EV} is calculated as

$$V_{EV} = -jQ_{EVDCS}\omega_{EVD}M_{EVD}I_{EVSC} \quad (3)$$

where Q_{EVDCS} is the quality factor of the EVDCS, ω_{EVD} and I_{EVSC} are the switching frequency and amplitude of the EVSC source current, respectively. It can be seen that V_{EV} is amplified by Q_{EVDCS} which normally ranges from tens to hundreds. When V_{EV} exceeds the pre-defined threshold, the Tx control unit will be notified of the approaching EV and start the Tx side. Since EVSC and EVDCS operate in a closed circuit, they are required to be decoupled with the Rx and Tx pads, respectively.

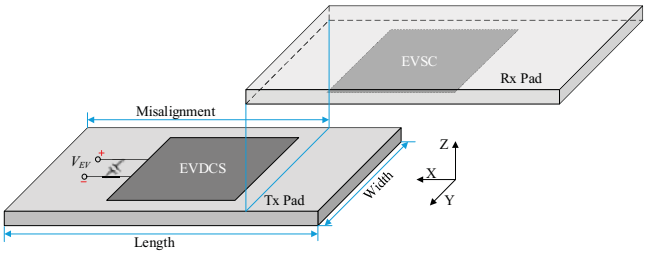

Fig. 3. EVD mechanisms

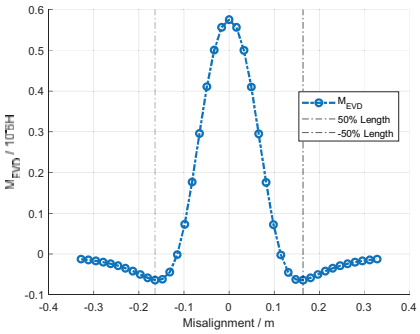

Fig. 4. Mutual inductance between EVSC and EVDCS

III. Design of the Proposed Detection System

The EVs and MFOs detection (EVFOD) system is designed for couplers using Double-D (DD) coil topology. The EVFOD system is composed of the EVSC in the Rx side and Tx detection coil sets (TDCSs) in the Tx side. TDCSs include both ACSs and PCSs.

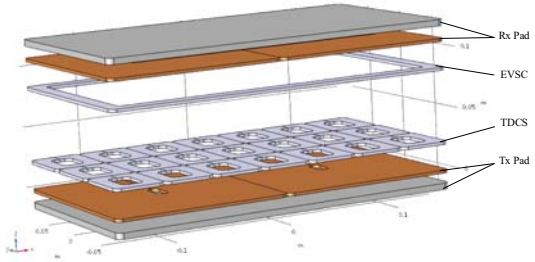

Fig. 5. Overveiw of the proposed EVFOD system for a DD coupler

A. PCSs coil design

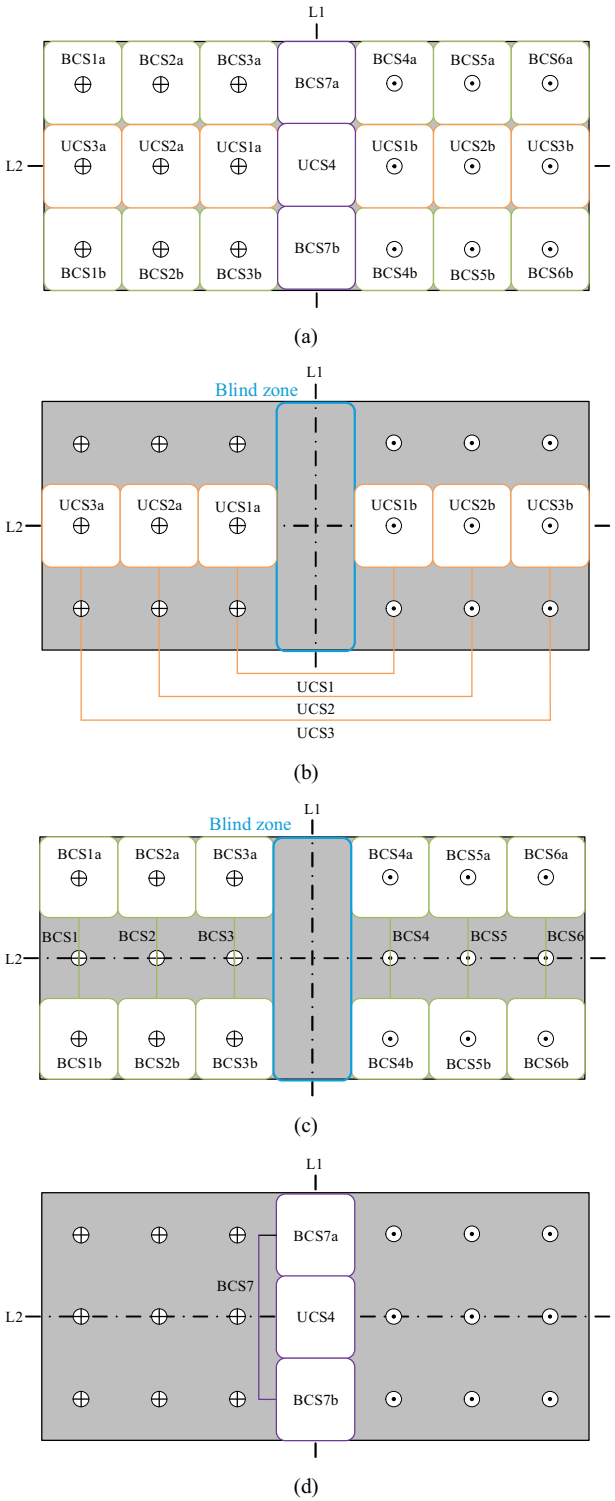

Fig. 6. EVFOD coil sets (a) overview, (b) and (c) PCSs, and (d) ACSs.

The PCS is required to be decoupled from the Tx pad to obtain a high S_{PCS}. According to the DD coil magnetic field property, the deployment of PCSs is illustrated in Fig. 5. Both unipolar coil sets (UCSs) and bipolar coil sets (BCSs) are adopted. UCSi (i = 1, 2 and 3) consists of two rectangular coils, UCSia and UCSib, which are arranged symmetrically at L1 and connected in opposing series. For example, UCS3 includes UCS3a and UCS3b. Since the magnetic flux produced by the Tx pad in UCS3a has the same amplitude and opposite direction with UCS3b, UCS3 is decoupled with the

Tx pad. Similarly, BCSi (i=1, 2, …, 6) is composed of two rectangular coils, BCSia and BCSib, placed symmetrically at L2 but connected in aiding series. For example, BCS1 includes BCS1a and BCS1b. The distributions of the magnetic field generated by the Tx pad are identical in the areas enclosed by the BCS1 and the BCS2. Therefore, BCSs are decoupled with the Tx pad as well. The proposed configuration gives access to using smaller rectangular coils to form detection coil sets, and a higher S_{PCS} can be achieved according to (1).

Based on the operation principle of PCSs, they can only detect MFOs when there is eddy current excited by the Tx pad. However, in the case that a planar MFO is placed symmetrically at L1, the magnetic flux within the area enclosed by the MFO could be zero, which means the MFO cannot be detected by PCSs.

B. ACSs coil design

In order to eliminate the blind zone shown in Fig. 6(b) and 6(c), the ACS detection method is adopted. ACSs include BCS7 and UCS4. UCS4 shares the same centre with the Tx pad, and BCS7a and BCS7b are symmetrical placed at L2. Thus, they are both decoupled with the Tx pad. According to the operation principles of ACSs, BCS7 and UCS4 are also required to be decoupled to simplify the resonant circuit design. This is naturally achieved by the proposed configuration. Since the EVDCS is also designed to be connected to a capacitor, it possible to apply BCS7 and UCS4 for FOD as well as EVD. Therefore, BCS7 and UCS4 are required to handle induced voltages caused by both MFOs and the EVSC. If the frequencies of the magnetic field produced by MFOs and the EVSC are different, these two induced voltages can be processed by the resonant circuits of the corresponding frequencies.

C. Resonant circuits design

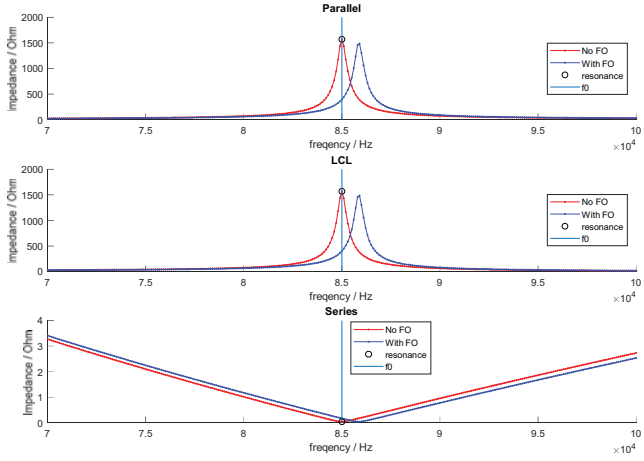

Fig. 7. Amplitude of the impedance for different resonances

The ACS detection method can be realized by parallel, series and LCL resonant circuits. The input impedance of the parallel, the LCL and the series resonant circuits are calculated in (4), where L_1 is fully compensated by C_1. Assuming there is a 5% decrement of self-inductance and increment of resistance, the amplitude of the input impedance in frequency domain is shown in Fig. 7. It can be seen that the parallel resonance is more sensitive and cost-effective. The input impedance of the parallel resonant circuit decreases to roughly one fourth when the MFO is presents.

$$\begin{cases} Z_p = \dfrac{j\omega L_1 + R_1}{-\omega^2 L_1 C_1 + j\omega\ {}_1R_1 + 1} \\ Z_{LCL} = \dfrac{j\omega L_1 + R_1}{-\omega^2 L_1 C_1 + j\omega\ {}_1R_1 + 1} + j\omega L_1 + R_1 \\ Z_s = j\omega L_1 + R_1 + \dfrac{1}{j\omega C_1} \end{cases} \quad (4)$$

FOD requires parallel capacitors to form a resonant circuit with ACSs, while EVD requires series capacitors. To satifsfy both requirements, this paper proposes a resonant circuit, named PPSP, enabling BCS7 and UCS4 to detect both MFOs and EVs, which is presented in Fig. 8(a). In order to distinguish the impacts of EVs and MFOs, the switching frequencies are designed to satisfy $\omega_{FOD} << \omega_{EVD}$. The capacitors are designed to satisfy the following requirements:

$$\begin{cases} C_{BCS} = \dfrac{1}{\omega_{EVD}{}^2 L_{BCS}} \\ C_{UCS} = \dfrac{1}{\omega_{EVD}{}^2 L_{UCS}} \\ C_p = \dfrac{1}{\omega_{FOD}{}^2 (L_{BCS} + L_{UCS4})} \end{cases} \quad (5)$$

When there is no induced voltage from the EVSC and the ACSs source V_{FOD} is supplying power, the PPSP circuit works in a low frequency mode as shown in Fig. 8(b). Since C_p is designed to compensate L_{BCS7} and L_{UCS4} at ω_{FOD}, self-inductance variation of BCS7 and UCS4 caused by the MFOs can result in a considerable decrement of the input impedance. As a result, the measured current for the FOD, I_d, increases and exceeds the predefined threshold, and the detection of the MFO can be achieved.

When the ACSs source V_{FOD} does not supply power and there is induced voltage from the EVSC, the PPSP circuit works in a high-frequency mode as shown in Fig. 8(c) and 8(d). In Fig. 8(c), the parallel resonant tank formed by L_{UCS4} and C_{UCS4} are in resonance at ω_{EVD}, and the input impedance is far larger than that of C_p and C_{BCS7} at ω_{EVD}. Therefore, the current through C_p is minimal, and L_{BCS7} forms a series resonance with C_{BCS7}. This series resonance makes the voltage across C_{BCS7} much higher than V_{EVD}, which is proved in (3). This principle also applies to the case shown in Fig. 8(d). The measured voltage for EVD, V_{EV}, is calculated as

$$V_{EV} = Q_{UCS4} V_{EVD,UCS4} + Q_{BCS7} V_{EVD,BCS7} \quad (6)$$

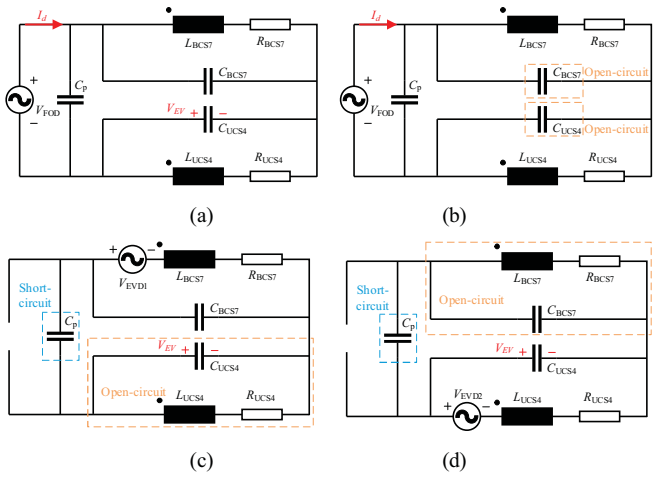

Fig. 8. PPSP resonant circuit and different mode, (a) PPSP topology, (b) low frequent mode, (c) and (d) high frequent mode.

When there is induced voltage from the EVSC and the ACSs source V_{FOD} is supplying power, UCS4 and BCS7 work for EVD and FOD simultaneously. There will be high-

frequency noise I_{ns} for I_d introduced from V_{EVD}, and low-frequency noise V_{ns} for V_{EV} caused by V_{FOD}. Since the parallel resonance provides a large input impedance when the coil quality factor is large, I_{ns} decays significantly. By selecting a proper V_{FOD}, I_{ns} could be negligible when compared to I_d. V_{ns} can be calculated as (7). In the comparison of (6) and (7), by keeping a high coil quality factor and V_{EV} could ensure that V_{ns} does not affect the feasibility of the EVD. Consequently, the operation of EVD and FOD can be realized at the same time.

$$V_{ns} \approx V_{FOD} \frac{L_{UCS4}}{L_{UCS4}+L_{BCS7}} \tag{7}$$

IV. Simulations

A. Sensitivity of detection coil sets

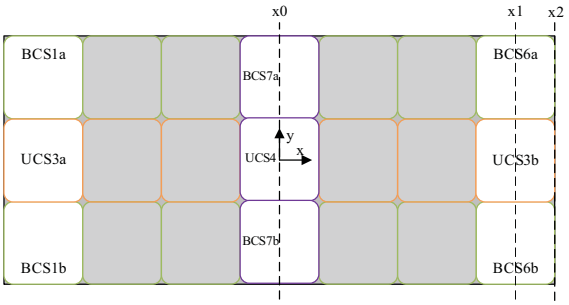

Fig. 9. Observed trajectories and coil sets

The EVFOD system is designed for a DD charging coupler with a length of 280 mm and width of 150 mm. The one euro coin, diameter of 23.25 mm and thickness of 2.33 mm, is taken as the reference MFO to test the sensitivity of the EVFOD coil sets. According to (1) and (2), the highest sensitivity can be attained when the size of the EVFOD coils is similar to the coin. However, the number of the EVFOD coil sets increases as the surface of the Tx pad has to be fully covered. Besides, more input channels of the controller are required. Therefore, the proposed EVFOD coils have a length of 42.6 mm and width 54.7 mm. The number of turns is selected to be 5 except for ACSs that have 10 turns to gain a higher self-inductance and mutual inductance with the EVSC.

The studied coil sets are presented in Fig. 9. One copper coin is placed along three trajectories x0, x1 and x2 to test the coil sets sensitivity. As BCS1, BCS6 and UCS3 are PCSs, the Tx pad is powered by a current with a peak of10 A. V_d of the studied coil sets is shown in Fig. 10. In both Fig. 10(a) and 10(b), UCS3 presents a higher sensitivity than BCS7, because the Tx pad magnetic field density is higher in the centre area. Beside, V_d of BCS6 and UCS3 peaks when the coin is placed in the centre of the detection coils. When the coin moves along x1, V_d can reach 0.4 V. By contrast, the peak value of V_d is 0.16 V at trajectory x2, less than half that of x1.

As the coin moves out of the area enclosed by the detection coils, the impact of the coin reduces. Therefore, weak points are located at the boundary of the detection coil. It can be seen that V_d at the boundaries 1 and 2 is relatively small. In Fig. 10(c), BCS7 has the largest V_d of 0.05 V. BCS7 and UCS4 demonstrate a similar sensitivity at trajectory x2 where the largest V_d is around 0.06 V. Although V_d is small at the boundaries 1 and 2, it is still enough for FOD.

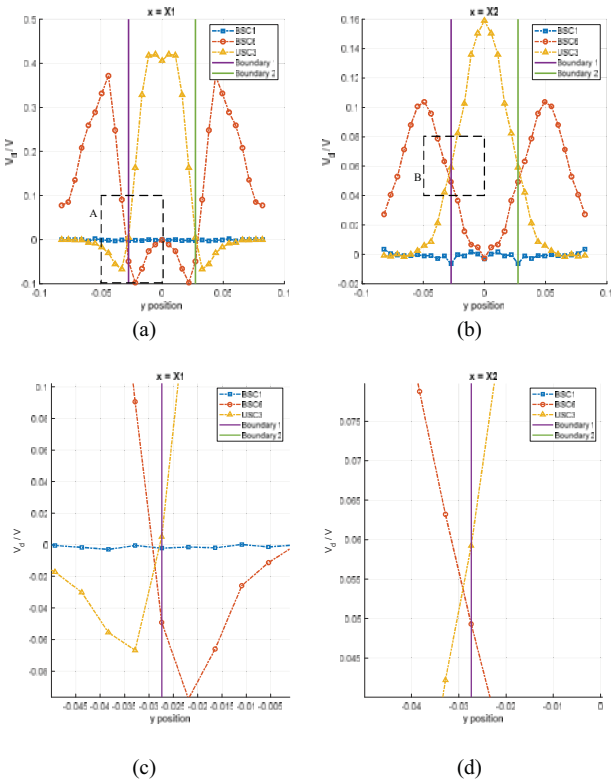

Fig. 10. Induced voltage of PCSs (a) x1, (b) x2, zoom-in pictures of (c) area A and (d) area B

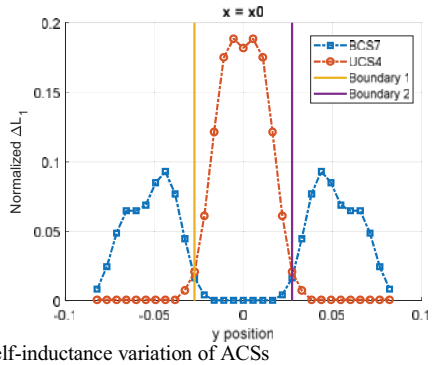

Fig. 11. Self-inductance variation of ACSs

The normalized variations of equivalent self-inductance ΔL_1 of BCS7 and UCS4 are illustrated in Fig. 11. ΔL_1 peaks when the coin locates around the centre of the detection coil sets. The peak value can be around 19% in UCS4. Similar to V_d of Fig. 10, when the coin is placed at the boundaries 1 and 2, ΔL_1 is around 2% which is much smaller than the peak value. Thanks to the proposed PPSP circuit, the variation of I_d caused by ΔL_1 can be amplified and detected.

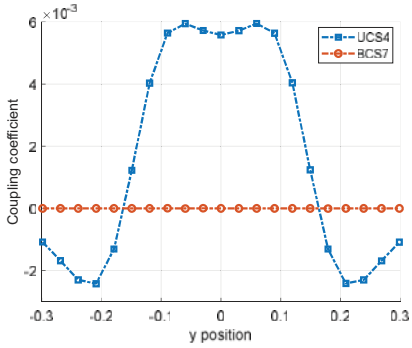

Fig. 12. Coupling between EVSC and ACSs

As the Rx pad also uses DD coil, the EVSC is designed to be a rectangular coil decoupled with the Rx pad. The coupling coefficient between ACSs and the EVSC, while the Rx pad moves along the centre of x-axis, is presented in Fig. 12. The coupling of BCS7 keeps zero since there is no y-axis misalignment and the magnetic flux in BCS7 stays at zero. The coupling of UCS4 peaks when Rx and Tx pads are nearly aligned. Although the peak coupling of UCS4 is small as 0.0056, the EVD series resonant circuit could simply amplify the induced voltage to an acceptable range, which is verified in the circuit simulations.

B. Feasibility of PPSP resonant circuits

TABLE I. PPSP CIRCUIT SPECIFICATIONS

Items	Value
L_{UCS4} / R_{UCS4}	5.96 μH / 0.1 Ω
L_{BCS7} / R_{BCS7}	9.92 μH / 0.1 Ω
f_{EVD} / f_{FOD}	1 MHz / 40 kHz
V_{FOD}	1 V
I_{EVSC}	0.26 A
k_{UCS4}	*0.0056*
$\Delta L_1/L_1$	*2%*

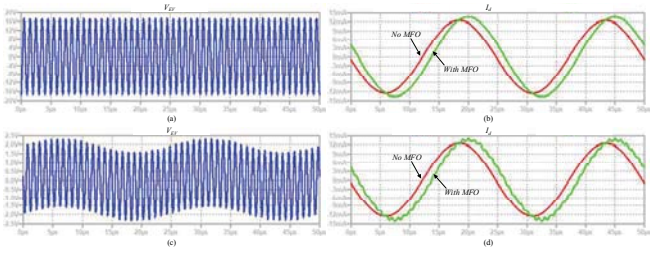

Fig. 13. PPSP circuit simulation (a) EVD alone when the EVSC is powered and aligned with the UCS4 and there is no MFO, (b) FOD alone when the EVSC is absent and there is a MFO, (c) and (d) EVFOD when EVSC is powered and aligned with the UCS4 and there is a MFO.

The circuit specifications are listed in Table I. The self-inductances are derived from the FEM model. The detection frequency of EVD f_{EVD} is 25 times as high as that of the FOD f_{EVD}, such that the PPSP circuit could distinguish the magnetic field of the ACSs from the EVSC. The coupling between UCS5 and EVSC k_{UCS4} and variation of coil self-inductance $\Delta L_1/L_1$ caused by the coin are set to be as 0.0056 and 2% to test the PPSP circuit performance.

The simulation results are presented in Fig. 13. In Fig. 13(a) , V_{EV} has a peak value of 17 V which is large enough for EVD. Compared with Fig. 13(a), the high frequency component of V_{EV} drops to 2 V due to the mistuning caused by the MFO. Although V_{EV} contains a 0.5 V low-frequency component, the high-frequency component is still 4 times larger and proves the feasibility of EVD.

In Fig. 13(b), the peak of I_d changes from 12.6 mA to 13.8 mA, suggesting a variation of 9.52% caused by a 2% self-inductance change. This variation remains the same in Fig. 13(d). The ripple resulted from the high frequency induced voltage of the ACSs is minimal and does not affect FOD.

V. CONCLUSION

This paper proposed an EVFOD system which applies the same detection coil sets to realize both EVD and FOD. The EVFOD system consists of detection coil sets and PPSP resonant circuit. The detection coil sets include both PCSs and ACSs to eliminate the blind zone and gain a high sensitivity to the intrusion of MFOs. The PPSP resonant circuit can further amplify the impact of MFOs and EVs to make EVFOD simple and reliable. Both FEM and circuit simulation models were built to verify the EVFOD system performance. The critical cases where a coin is placed on the weak points of the detection coil sets were also analysed. The results proves the sensitivity of the proposed coil sets and the feasibility of the proposed PPSP resonant circuits.

REFERENCES

[1] K. Lee, Z. Pantic, and S. M. Lukic, "Reflexive Field Containment in Dynamic Inductive Power Transfer Systems," *IEEE Transactions on Power Electronics*, vol. 29, no. 9, pp. 4592–4602, Sep. 2014.

[2] G. R. Nagendra, L. Chen, G. A. Covic, and J. T. Boys, "Detection of EVs on IPT Highways," *IEEE Journal of Emerging and Selected Topics in Power Electronics*, vol. 2, no. 3, pp. 584–597, Sep. 2014.

[3] S. Fukuda, H. Nakano, Y. Murayama, T. Murakami, O. Kozakai, and K. Fujimaki, "A novel metal detector using the quality factor of the secondary coil for wireless power transfer systems," in *2012 IEEE MTT-S International Microwave Workshop Series on Innovative Wireless Power Transmission: Technologies, Systems, and Applications*, 2012, pp. 241–244.

[4] H. Kikuchi, "Metal-loop effects in wireless power transfer systems analyzed by simulation and theory," in *2013 IEEE Electrical Design of Advanced Packaging Systems Symposium (EDAPS)*, 2013, pp. 201–204.

[5] N. Kuyvenhoven, C. Dean, J. Melton, J. Schwannecke, and A. E. Umenei, "Development of a foreign object detection and analysis method for wireless power systems," in *2011 IEEE Symposium on Product Compliance Engineering Proceedings*, 2011, pp. 1–6.

[6] C. T. Rim and C. Mi, "Foreign Object Detection," in *Wireless Power Transfer* for *Electric Vehicles and Mobile Devices*, IEEE, 2017.

[7] S. Y. Jeong, H. G. Kwak, G. C. Jang, S. Y. Choi, and C. T. Rim, "Dual-Purpose Nonoverlapping Coil Sets as Metal Object and Vehicle Position Detections for Wireless Stationary EV Chargers," *IEEE Transactions on Power Electronics*, vol. 33, no. 9, pp. 7387–7397, Sep. 2018.

[8] S. Verghese, M. P. Kesler, K. L. Hall, and H. T. Lou, "Foreign object detection in wireless energy transfer systems," US9442172B2, 13-Sep-2016.

[9] L. Xiang, Z. Zhu, J. Tian, and Y. Tian, "Foreign Object Detection in a Wireless Power Transfer System Using Symmetrical Coil Sets," *IEEE Access*, vol. 7, pp. 44622–44631, 2019.

[10] S. Y. Jeong, V. X. Thai, J. H. Park, and C. T. Rim, "Self-Inductance-Based Metal Object Detection With Mistuned Resonant Circuits and Nullifying Induced Voltage for Wireless EV Chargers," *IEEE Transactions on Power Electronics*, vol. 34, no. 1, pp. 748–758, Jan. 2019.

[11] V. X. Thai, G. C. Jang, S. Y. Jeong, J. H. Park, Y.-S. Kim, and C. T. Rim, "Symmetric Sensing Coil Design for the Blind-zone Free Metal Object Detection of a Stationary Wireless Electric Vehicles Charger," *IEEE Transactions on Power Electronics*, pp. 1–1, 2019.

[12] W. Shi, J. Dong, S. Bandyopadhyay, F. Grazian, T. B. Soeiro, and P. Bauer, "Comparative Study of Foreign Object and Misalignment in Inductive Power Transfer Systems," in *IECON 2019 - 45th Annual Conference of the IEEE Industrial Electronics Society*, 2019, vol. 1, pp. 2634–2639.